Molecular hydrogen and catalytic combustion in the production of hyperpolarized ^{83}Kr and ^{129}Xe MRI contrast agents

Nicola J. Rogers[a,1], Fraser Hill-Casey[a,b], Karl F. Stupic[a,2], Joseph S. Six[a,3], Clémentine Lesbats[a], Sean P. Rigby[b], Jacques Fraissard[c], Galina E. Pavlovskaya[a], and Thomas Meersmann[a,4]

[a]Sir Peter Mansfield Imaging Centre, Division of Respiratory Medicine, School of Medicine, University of Nottingham, Nottingham NG7 2RD, United Kingdom; [b]Department of Chemical and Environmental Engineering, University of Nottingham, Nottingham NG7 2RD, United Kingdom; and [c]Ecole Supérieure de Physique et Chimie Industrielles, Université Pierre et Marie Curie, 75005 Paris, France

Edited by Alexis T. Bell, University of California, Berkeley, CA, and approved January 29, 2016 (received for review January 11, 2016)

Hyperpolarized (hp) ^{83}Kr is a promising MRI contrast agent for the diagnosis of pulmonary diseases affecting the surface of the respiratory zone. However, the distinct physical properties of ^{83}Kr that enable unique MRI contrast also complicate the production of hp ^{83}Kr. This work presents a previously unexplored approach in the generation of hp ^{83}Kr that can likewise be used for the production of hp ^{129}Xe. Molecular nitrogen, typically used as buffer gas in spin-exchange optical pumping (SEOP), was replaced by molecular hydrogen without penalty for the achievable hyperpolarization. In this particular study, the highest obtained nuclear spin polarizations were $P = 29\%$ for ^{83}Kr and $P = 63\%$ for ^{129}Xe. The results were reproduced over many SEOP cycles despite the laser-induced on-resonance formation of rubidium hydride (RbH). Following SEOP, the H_2 was reactively removed via catalytic combustion without measurable losses in hyperpolarized spin state of either ^{83}Kr or ^{129}Xe. Highly spin-polarized ^{83}Kr can now be purified for the first time, to our knowledge, to provide high signal intensity for the advancement of in vivo hp ^{83}Kr MRI. More generally, a chemical reaction appears as a viable alternative to the cryogenic separation process, the primary purification method of hp ^{129}Xe for the past 2 1/2 decades. The inherent simplicity of the combustion process will facilitate hp ^{129}Xe production and should allow for on-demand continuous flow of purified and highly spin-polarized ^{129}Xe.

spin-exchange optical pumping | hyperpolarized noble gas contrast agents | cryogenic separation | chemical looping combustion | pulmonary imaging

The development of hyperpolarized (hp) noble gas MRI has resulted in a number of excellent protocols to probe different structural and functional aspects of lungs in health and disease (1–6). Technological improvements (6–15) have enabled pulmonary hp ^{129}Xe MRI at high spatial resolution, thereby reducing the need for use of the scarcely available ^{3}He isotope. Furthermore, tissue solubility, large chemical shift range, and interaction with specific sensor molecules allow for a variety of hp ^{129}Xe applications in biomedical sciences and beyond (1–6, 16, 17). Despite its nuclear electric quadrupole moment that causes rapid relaxation, the isotope ^{83}Kr (nuclear spin $I = 9/2$) can be hyperpolarized through Rb spin-exchange optical pumping (SEOP) as first demonstrated by Grover (18) and explored in detail by Happer and coworkers (19). Volk et al. first observed ^{83}Kr quadrupolar coupling in the gas phase that originated from the surface of the SEOP cell (20), and Mehring and coworkers described T_2 relaxation as a probe for the cell surfaces (21). The intriguing properties of ^{83}Kr can be more generally used after the removal of the reactive Rb vapor to generate surface-sensitive MRI contrast (22). Most recently, T_1 surface quadrupolar relaxation MRI contrast (23) with hp ^{83}Kr in excised lungs was demonstrated to be indicative of surface-to-volume changes in an animal model of emphysema (24).

Although hp ^{129}Xe can be obtained through dynamic nuclear polarization (25) with high spin-polarization levels of up to $P = 30\%$ (26), at present only SEOP can produce hp ^{129}Xe with $P \geq 90\%$. Furthermore, SEOP is currently the only method to provide hp ^{83}Kr for biomedical MRI applications (24). During SEOP of ^{83}Kr or ^{129}Xe, the noble gas is diluted with a buffer gas, usually either a ^{4}He–N_2 mixture or pure N_2 gas. The buffer gas serves a dual purpose as it prevents destructive radiation trapping, originating from radiative electronic relaxation of rubidium (27, 28), but also causes pressure broadening of the Rb D_1 linewidth. Rubidium line broadening maximizes adsorption of laser light emitted by high-power solid devices, even if those are line narrowed. Following SEOP, hp ^{129}Xe is cryogenically separated from the gas mixture under carefully chosen conditions to prevent polarization loss (29). Cryogenic separation complicates the operational procedures for clinical and preclinical hp ^{129}Xe MRI. For a number of applications a repeat noble gas delivery at high polarization and concentration levels is needed (6, 30–35). Additionally, a very constant level of spin polarization is required for molecular imaging with hp ^{129}Xe biosensors using the hyperpolarized xenon chemical exchange saturation transfer (HyperCEST) methodology (17, 36–38). Cryogenic separation enables increased polarization in pure xenon gas but is inherently a "batch mode" production

Significance

The high signal intensity associated with magnetic resonance of hyperpolarized ^{129}Xe has enabled countless applications ranging from materials science to biomedical MRI of the lung and brain. New modalities are constantly emerging; for example, hyperpolarized ^{129}Xe biosensors are of potential interest for molecular imaging of biomarker distribution in organs. Hyperpolarized ^{83}Kr shows promise as novel surface-sensitive contrast agent for pulmonary MRI but previous work was limited to excised lungs. This work reports a previously unexplored approach in the generation of hyperpolarized contrast agents that makes highly concentrated hyperpolarized ^{83}Kr available for the first time, to our knowledge. The results also provide the basis for on-demand flow production of highly concentrated hyperpolarized ^{129}Xe for in situ process monitoring and in vivo molecular imaging.

Author contributions: T.M. conceived the general concept of reactive buffer gas removal; N.J.R., S.P.R., J.F., G.E.P., and T.M. designed research; F.H.-C. and K.F.S. performed spin-exchange optical pumping (SEOP) experiments; F.H.-C. and J.S.S. recorded IR data; N.J.R. and C.L. conducted combustion research; and T.M. wrote the paper.

The authors declare no conflict of interest.

This article is a PNAS Direct Submission.

[1]Present address: Department of Chemistry, Durham University, Durham DH1 3LE, United Kingdom.

[2]Present address: Physical Measurement Laboratory, National Institute of Standards and Technology, Boulder, CO 80305.

[3]Present address: Carestream Health Inc., White City, OR 97503.

[4]To whom correspondence should be addressed. Email: Thomas.Meersmann@Nottingham.ac.uk.

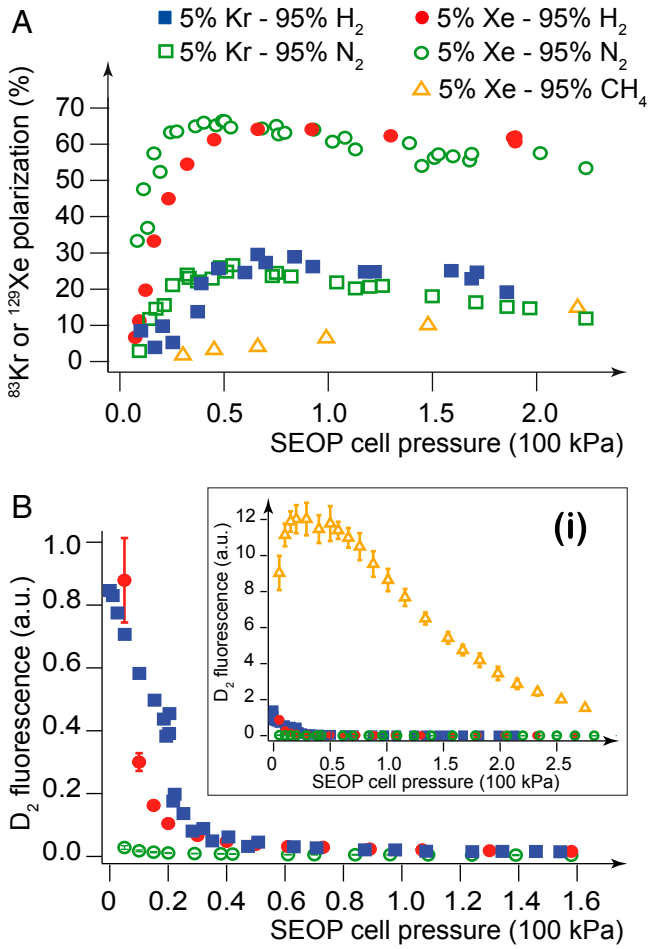

Fig. 1. (*A*) SEOP-generated ^{129}Xe and ^{83}Kr spin polarization in mixtures containing 5% noble gas and 95% buffer gas as a function of total SEOP gas pressure. Using H_2 as buffer gas, the ^{129}Xe spin polarization (obtained at 378 K) is shown in red filled circles and the ^{83}Kr polarization (obtained at 440 K) is displayed as blue filled squares. For comparison, previous data from ref. 39 with N_2 as buffer gas is shown for ^{129}Xe SEOP at 378 K (green open circles) and for ^{83}Kr SEOP at 433 K (green open squares). In contrast, CH_4 is an inefficient buffer gas that led to low spin polarization (orange open triangles, taken from ref. 54). (*B*) The D_2 fluorescence at 780 nm (in arbitrary units, a.u.) measured at the front of the cell during SEOP indicates that sufficient radiation quenching with H_2 at 378 K (red circles) and at 433 K (blue squares) requires pressures above 50 kPa. Using N_2 (green open circles), the D_2 radiation is efficiently quenched at pressures above ~5 kPa. *Inset* (*i*) shows the high D_2 fluorescence measured for Xe SOEP at 378 K with methane that is a very ineffective quenching gas.

process that disrupts on-demand continuous flow. Whereas cryogenic separation may complicate and limit some hp ^{129}Xe applications, it is not an option at all for the hp ^{83}Kr production due to the fast quadrupolar relaxation. To avoid cryogenic separation, SEOP at a high noble gas mole fraction has been explored in the past (6, 10, 14, 39–41). Nevertheless, gas dilution is still required to ensure high spin polarization at the high production volumes required for MRI and the dilution therefore reduces MRI signal intensity per unit volume of inhaled gas. An innovative method developed by Kimura, Imai, Fujiwara, and coworkers (6, 10, 33) produces a constant stream of 70% concentrated hp ^{129}Xe but the polarization is typically in the $P = 10\%$ regime. In this work, ^{129}Xe and ^{83}Kr SEOP is attempted with mixtures containing molecular hydrogen as buffer gas and radiation quenching agent (42–46) that can subsequently be removed through catalytic combustion.

Results and Discussions

Fig. 1*A* shows the ^{129}Xe nuclear spin polarization, P, as a function of gas pressure after 6 min of SEOP of a mixture of 5% Xe and 95% Kr at an external cell temperature of 378 K. The spin polarization is similar to data produced previously with a 5% Xe–95% N_2 mixture under almost identical conditions described and analyzed in detail in ref. 39, also shown in Fig. 1*A* for comparison. Using H_2 buffer gas, hp ^{129}Xe with up to $P = 63\%$ was generated within 6 min of SEOP at 70 kPa total gas pressure. Using 5% krypton in 95% buffer gas, the highest ^{83}Kr polarization of $P = 29\%$, obtained with H_2 after 11 min of SEOP at 440 K, is comparable to that obtained previously with N_2 under similar conditions (39).

On-Resonance Rubidium Hydride Formation. The high spin-polarization values for ^{83}Kr with the H_2 in Fig. 1*A* were achieved repeatedly for more than 30 h of SEOP over a time span of about 1 wk and for ^{129}Xe over a duration of at least 6 h of continuous SEOP despite the formation of rubidium hydrides (RbH) during on-resonance D_1 laser irradiation (47). Over time. a white RbH

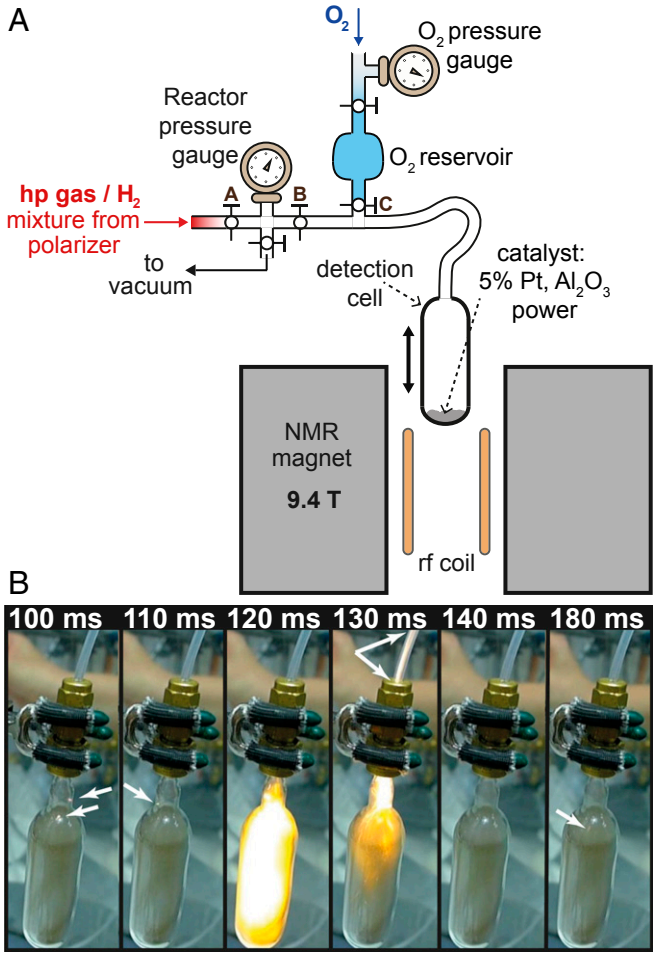

Fig. 2. (*A*) Experimental setup used for combustion experiments. Using pressure equalization, the hp gas/H_2 mixture was shuttled to the reactor/detection cell containing the Pt catalyst. Oxygen was then injected from the O_2 reservoir. (*B*) Exported pictures from 100 frame per second video of the reactor upon O_2 delivery. Approximately 100 ms after opening of valve C, minor combustion zones became visible (see white arrows), indicating that the catalytic oxidation of the H_2 gas had commenced. The major combustion event took place 20–30 ms thereafter and the combustion appeared to be largely completed within 80 ms. The reactor outside temperature increase was limited to approximately 5 K.

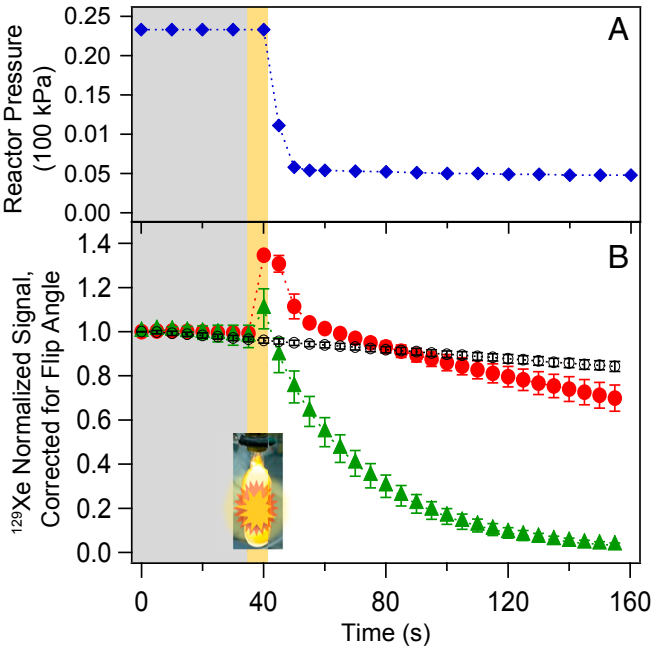

Fig. 3. (*A*) In situ reactor pressure measurements (blue diamonds) during the combustion reaction of a 5% Xe/95% H_2 gas mixture, with oxygen reservoir tap (tap C, Fig. 2*A*) opened at $t = 40$ s adding 11.2 ± 0.4 kPa partial pressure of O_2. Average initial partial pressure of H_2 = 22.0 ± 1 kPa and the oxygen addition caused the pressure drop due to the combustion reaction (a short term pressure increase, if present, was not observed at the time resolution of the gauge). (*B*) NMR measurements performed in separate experiments without pressure gauge (i.e., tap B, Fig. 2*A* was kept shut to reduce the dead volume of the experiment). Normalized integrated hp ^{129}Xe NMR signals following a 9° pulse during the catalytic oxidation with 13.4 ± 0.4 kPa oxygen (red circles) or 20.5 ± 0.5 kPa (green triangles) added at $t = 40$ s. Average initial partial pressure of H_2 = 25.5 ± 1 kPa. Control signals with no oxygen/combustion (tap C, Fig. 2*A*, remained closed) shown as black open circles. Signal intensity data were corrected for flip-angle attenuation and are the average from three repeat measurements.

deposition was observed on all SEOP cell surfaces but to a lesser extent at the laser entry window. Furthermore, SEOP cell recycling, causing substantial removal of the RbH, was possible by increasing the temperature to 480 K for about 30 min with ongoing laser irradiation while the cell was connected, via a Rb trap, to a vacuum pump. Although excessive RbH buildup on the cell entry window will reduce laser irradiation, deposition on other cell surfaces may not necessarily adversely affect the achievable noble gas spin polarization. Previous work demonstrated that the ^{131}Xe T_1 relaxation time increases for this spin $I = 3/2$ isotope because of RbH buildup (48–50). RbH surface coating may therefore also reduce the ^{83}Kr T_1 relaxation rates and improve SEOP. A detailed study by Cates and coworkers explored the effect of RbH surface deposition on the T_1 relaxation of ^{129}Xe as a function of field strength (≥0.08 T) and temperature (≤340 K) in a spherical 25-mm-diameter cell (51). Based on the results one may interpolate ^{129}Xe T_1 times in excess of 400 s at the conditions used in the current work, causing little interference during rapid SEOP.

H_2 as Radiation Quenching Agent. The high polarization values obtained with H_2 in Fig. 1*A*, i.e., in the absence of any N_2, are remarkable. Depending on SEOP temperature, the gas mixtures usually contain at least a partial pressure of 5 kPa of molecular nitrogen for radiation quenching to prevent radiation trapping of arbitrarily polarized fluorescence photons that severely reduce Rb polarization (27, 28). Previous work investigating the efficacy of H_2 to quench Rb radiation found that the effective cross-sections for quenching of the D_1 and D_2 transitions are about 1 order of magnitude smaller for H_2 than for N_2 (42). An empirical model of radiation quenching with H_2 is reported in ref. 52 but is limited to buffer gas pressures below 7 kPa. Generally, H_2 has found little consideration as quenching agent at high gas density and temperature conditions typically used for SEOP production of hp ^{129}Xe or hp ^{83}Kr for MRI applications.

The measurement of D_1 fluorescence at 795 nm, obscured by high-power laser radiation, is experimentally very demanding. Instead, the Rb D_2 fluorescence during SEOP was straightforwardly monitored in this work. The mixing cross-sections between the electronic states Rb*$5^2P_{1/2}$ and Rb*$5^2P_{3/2}$ are comparable for H_2 and N_2 (42) and the D_2 fluorescence should therefore provide at least qualitative insights into D_1 radiation quenching efficiency of the molecular hydrogen. Fig. 1*B* demonstrates that H_2 serves as a remarkably efficient radiation quenching agent at partial pressures above ∼40–60 kPa, where little fluorescence was detected during SEOP even at the very high temperature of 433 K. Therefore, H_2 can be used as radiation quenching agent during SEOP but the required partial pressure is about 10 times higher than that for N_2, in agreement with previous measurements of quenching cross-section in ref. 42. Below this critical partial pressure, radiation quenching is largely incomplete and a substantial difference in the D_2 fluorescence is observed between SEOP of ^{129}Xe and ^{83}Kr. Fig. 1*B* depicts a higher fluorescence count at the elevated temperature used for ^{83}Kr SEOP (in the 433–440-K range) where the Rb density is almost 20-fold increased compared with that for ^{129}Xe SEOP at 378 K. At low buffer gas pressure, where radiation quenching is incomplete, the high Rb density for ^{83}Kr SEOP produces significantly more radiation trapping. The consequences of the increased radiation trapping can be

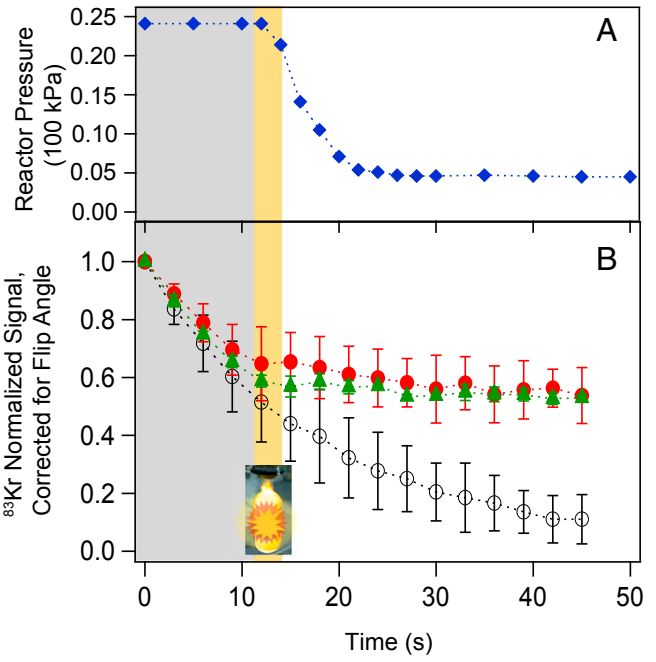

Fig. 4. (*A*) Pressure curve of combustion reaction of a 5% Kr/95% H_2 gas mixture with 11.2 ± 4 kPa O_2 added after 12 s causing the reaction and observed pressure drop. Average initial partial pressure of H_2 = 23.5 ± 1 kPa. (*B*) Normalized integrated hp ^{83}Kr NMR signals following a 12° pulse during the combustion reaction adding 13.4 ± 0.4 kPa (red circles) and 20.5 ± 0.5 kPa (green triangles) partial pressure of oxygen. Average initial partial pressure of H_2 = 27.5 ± 2.5 kPa. Black open circles show control signals for a 5% Kr/95% H_2 gas mixture with no combustion. Signal intensity data were corrected for flip-angle attenuation and are the average from three repeat measurements.

observed in Fig. 1*A* where, at buffer gas pressures below ~50 KPa, the noble gas polarization obtained through SEOP with H_2 falls short compared with that with N_2. The effect of Rb density on radiation trapping was previously studied at extremely low H_2 partial pressure (<0.1Pa) for the purpose of SEOP of dissociated atomic hydrogen (43–46). Under these conditions, radiation quenching is effectively nonexistent and radiation trapping can be limited only by keeping the Rb densities very low through SEOP temperatures around or below 318 K. In the current work, no adverse effect of H_2 as buffer gas at SEOP pressures above 40–50 kPa (with the exception of reversible RbH formation, discussed above) was found compared with SEOP with N_2 under otherwise identical conditions, regardless of the temperature. Note that the high IR quenching cross-section of H_2 is a rare exception among small molecules without chemical double or triple bonds and Fig. 1 includes data obtained with CH_4 as buffer gas for comparison. The inefficient small quenching cross-section of CH_4 (53) causes a high IR count (Fig. 1*B*) and a correspondingly low ^{129}Xe spin polarization below that of hp ^{83}Kr (Fig. 1*A*), a problem that was previously solved using a ternary mixture of 5% Xe, 85% CH_4, and 10% N_2 (54).

Buffer Gas Removal Through Catalytic Combustion. Efficient SEOP of noble gases in H_2 mixtures opens a path for oxidative buffer gas elimination that produces H_2O as the only reaction product. Most of the generated water vapor can straightforwardly be removed through condensation at ambient temperature. The resulting gas phase is composed of the purified hp noble gas in addition to a small remaining quantity of the water vapor. Previous work demonstrated qualitatively the feasibility of hp ^{129}Xe MRI (54) of a methane combustion zone. To quantify the effect of catalytic hydrogen combustion on the noble gas spin polarization, an experimental setup was devised as sketched in Fig. 2*A*. Shuttling of hp noble gas–H_2 mixture into the reactor chamber that contained a small quantity of Pt and monitoring the signal decay over time through NMR spectroscopy at 9.4 T provided the baseline data, shown as open circles in Fig. 3*B*, for hp ^{129}Xe and in Fig. 4*B* for hp ^{83}Kr. For oxidative H_2 removal, O_2 was added, which led to hydrogen combustion within <100 ms due to the presence of the Pt catalyst, as depicted in Fig. 2*B*. The reactor pressure during this process was monitored (Figs. 3*A* and 4*A*) but potential short pressure increases during the reaction were not detected at the time resolution of the pressure gauge. Upon adding O_2, slightly above the stoichiometric ratio, the pressure decreased within 15 s as the sole reaction product, H_2O, had condensed rapidly upon cooling. The temperature increase measured outside the reactor was limited to 5 K and the final reactor pressure of 4.7 ± 0.5 kPa was close to that expected from the combined water vapor pressure at ambient temperature (3.2 kPa at 298 K) and the noble gas partial pressure (1.2–1.3 kPa).

Monitoring the hp ^{129}Xe signal intensity (Fig. 3*B*), an initial signal increase was observed upon O_2 delivery, caused by hp ^{129}Xe influx from the connecting tubing [i.e., perfluoroalkoxy polymer (PFA) tubing with 1.6-mm inner diameter] that was pushed into the reaction chamber by the oxygen gas. Within 20 s, gas convection and diffusion returned the signal intensity approximately to the baseline value, indicating that the nuclear spin state had experienced no significant depolarization. However, after the reaction, the ^{129}Xe relaxation was accelerated due to a small excess of paramagnetic O_2 (approximately 0.7 kPa partial pressure). Increasing the O_2 excess to 7.5 ± 0.5 kPa led to further accelerated ^{129}Xe signal decay.

The hp ^{83}Kr data in Fig. 4*B* demonstrate that combustion caused no signal loss and, in contrast to ^{129}Xe, the ^{83}Kr gas-phase relaxation slowed down after the reaction. The decrease of the ^{83}Kr T_1 relaxation was likely a consequence of competitive coadsorption of water molecules on the reactor surface that have been found previously to reduce krypton surface interactions (55). The very low gyromagnetic ratio makes ^{83}Kr insensitive to paramagnetic relaxation even at higher (7.5 ± 0.5 kPa) oxygen partial pressure (Fig. 4*B*) (40). An initial short-term signal increase upon O_2 gas delivery, present in the ^{129}Xe data, was not observed because hp ^{83}Kr located in the connecting PFA tubing depolarized due to fast quadrupolar T_1 relaxation in the presence of the fluorocarbon surface (56).

Conclusion

The capability to almost instantaneously remove a buffer gas that serves as an efficient radiation quenching agent during SEOP allows, for the first time to our knowledge, for the generation of purified, highly spin-polarized ^{83}Kr. Furthermore, the method may be of interest for a fully automated hp ^{129}Xe production at reduced costs without the need for cryogenic operations. Because of the low total gas pressure after catalytic buffer gas removal, the hp gases will require recompression to ambient pressure for biomedical application. Recompression has previously been demonstrated with little polarization loss for hp ^{129}Xe (10, 40) and acceptable 1/4 polarization loss for hp ^{83}Kr (40). Based on the result in this work, this would suggest that purified hp ^{83}Kr with 21% spin polarization is now feasible, a sevenfold improvement over recent hp ^{83}Kr work with 3% apparent polarization that already allowed for MRI with 0.795 × 0.635-mm^2 resolution in ex vivo lungs (24).

Note that the experimental setting was for the sole purpose of proof of concept demonstration and can be substituted by combustion under continuous flow within a catalytic converter. Furthermore, direct contact between H_2 and O_2 may be avoidable through the use of recyclable metal oxides similar to those used in chemical looping combustion (57). Reactive H_2 removal may take place in a small flow-through catalytic converter placed downstream from the SEOP cell that would facilitate gas transport through the generated pressure gradient. Kimura, Imai, Fujiwara, and coworkers used a peristaltic pump for continuous hp ^{129}Xe recompression after continuous flow SEOP at low pressures (6, 10, 33), a concept that could be further extended by flow-through catalytic buffer gas removal before recompression. Enabling on-demand production of an uninterrupted, continuous flow of hp ^{129}Xe at high spin polarization and purity, this concept should be of high value for a variety of applications ranging from material science to biomedical MRI. If required, hp ^{129}Xe could also be stored before recompression (and even before H_2 removal), using the extraordinary slow T_1 relaxation of ^{129}Xe described in the past for gas phase xenon under certain conditions (58–60). As a final note, the presented concept does not involve any toxic reagents or reaction products and the complete absence of nitrogen and carbon prevents any accidental generation of nitrogen oxides (NO_x) and carbon monoxide (CO) during combustion. Any H_2 passing through the "buffer gas removal step," however unlikely, can straightforwardly be detected through reliable hydrogen microsensors.

Materials and Methods

SEOP was conducted at 0.04-T field strength in a 75-cm^3 cylindrical borosilicate cell (~120 mm long, 28-mm inner diameter) using a Comet module (Spectra Physics) laser with a 0.25-nm linewidth producing 23-W incident power at the SEOP cell entrance window under very similar conditions as described in detail in ref. 39. A mixture of 5% Xe (or 5% Kr) in H_2 was used for all experiment in this work with natural abundance noble gas isotope distribution (i.e., 26.4% ^{129}Xe and 11.5% ^{83}Kr). Spin polarization was determined as described in ref. 39 (see also ref. 6) and a general expression for polarization of $I \geq 1/2$ spin systems is discussed in ref. 61. To monitor the Rb D_2 fluorescence during SEOP at 780 nm, an HR2000+ Ocean Optics spectrometer was used.

All catalytic combustion experiments took place in a 1.5-mm glass wall vessel that contained 25 mg Pt/Al_2O_3 catalyst powder (i.e., 5 wt % dry loading Pt on alumina). Standard safety precautions were followed and the H_2–hp noble gas mixture was delivered to the reactor at pressures below 30 kPa to limit temperature and pressure bursts that could compromise reactor integrity. The reactor pressure was metered using a gas composition independent diaphragm gauge (OmegaDYNE Inc.).

ACKNOWLEDGMENTS. We thank Colin E. Snape for stimulating discussions. This work was supported in part by the Medical Research Council under Grant G0900785 and by the Royal Society through the Paul Instrument Fund.

1. Mugler JP, 3rd, Altes TA (2013) Hyperpolarized 129Xe MRI of the human lung. *J Magn Reson Imaging* 37(2):313–331.
2. Lilburn DML, Pavlovskaya GE, Meersmann T (2013) Perspectives of hyperpolarized noble gas MRI beyond 3He. *J Magn Reson* 229:173–186.
3. Liu Z, Araki T, Okajima Y, Albert M, Hatabu H (2014) Pulmonary hyperpolarized noble gas MRI: Recent advances and perspectives in clinical application. *Eur J Radiol* 83(7):1282–1291.
4. Walkup LL, Woods JC (2014) Translational applications of hyperpolarized 3He and 129Xe. *NMR Biomed* 27(12):1429–1438.
5. Ruppert K (2014) Biomedical imaging with hyperpolarized noble gases. *Rep Prog Phys* 77(11):116701.
6. Meersmann T, Brunner E, eds (2015) *Hyperpolarized Xenon-129 Magnetic Resonance* (Royal Society of Chemistry, Cambridge, UK).
7. Driehuys B, et al. (1996) High-volume production of laser-polarized Xe-129. *Appl Phys Lett* 69(12):1668–1670.
8. Ruset IC, Ketel S, Hersman FW (2006) Optical pumping system design for large production of hyperpolarized. *Phys Rev Lett* 96(5):053002.
9. Hersman FW, et al. (2008) Large production system for hyperpolarized 129Xe for human lung imaging studies. *Acad Radiol* 15(6):683–692.
10. Imai H, Fukutomi J, Kimura A, Fujiwara H (2008) Effect of reduced pressure on the polarization of Xe-129 in the production of hyperpolarized Xe-129 gas: Development of a simple continuous flow mode hyperpolarizing system working at pressures as low as 0.15 atm. *Concepts Magn Reson Part B Magn Reson Eng* 33B(3):192–200.
11. Schrank G, Ma Z, Schoeck A, Saam B (2009) Characterization of a low-pressure high-capacity 129Xe flow-through polarizer. *Phys Rev A* 80(6):063424.
12. Mugler JP, 3rd, et al. (2010) Simultaneous magnetic resonance imaging of ventilation distribution and gas uptake in the human lung using hyperpolarized xenon-129. *Proc Natl Acad Sci USA* 107(50):21707–21712.
13. Norquay G, Parnell SR, Xu XJ, Parra-Robles J, Wild JM (2013) Optimized production of hyperpolarized Xe-129 at 2 bars for in vivo lung magnetic resonance imaging. *J Appl Phys* 113(4):044908.
14. Nikolaou P, et al. (2013) Near-unity nuclear polarization with an open-source 129Xe hyperpolarizer for NMR and MRI. *Proc Natl Acad Sci USA* 110(35):14150–14155.
15. Freeman MS, Emami K, Driehuys B (2014) Characterizing and modeling the efficiency limits in large-scale production of hyperpolarized (129)Xe. *Phys Rev A* 90(2):023406.
16. Spence MM, et al. (2001) Functionalized xenon as a biosensor. *Proc Natl Acad Sci USA* 98(19):10654–10657.
17. Schröder L, Lowery TJ, Hilty C, Wemmer DE, Pines A (2006) Molecular imaging using a targeted magnetic resonance hyperpolarized biosensor. *Science* 314(5798):446–449.
18. Grover BC (1978) Noble-gas NMR detection through noble-gas-rubidium hyperfine contact interaction. *Phys Rev Lett* 40(6):391–392.
19. Schaefer SR, Cates GD, Happer W (1990) Determination of spin-exchange parameters between optically pumped rubidium and 83Kr. *Phys Rev A* 41(11):6063–6070.
20. Volk CH, Mark JG, Grover BC (1979) Spin dephasing of Kr-83. *Phys Rev A* 20(6): 2381–2388.
21. Butscher R, Wäckerle G, Mehring M (1996) Nuclear quadrupole surface interaction of gas phase Kr-83: Comparison with Xe-131. *Chem Phys Lett* 249(5-6):444–450.
22. Pavlovskaya GE, Cleveland ZI, Stupic KF, Basaraba RJ, Meersmann T (2005) Hyperpolarized krypton-83 as a contrast agent for magnetic resonance imaging. *Proc Natl Acad Sci USA* 102(51):18275–18279.
23. Six JS, et al. (2014) Pulmonary MRI contrast using Surface Quadrupolar Relaxation (SQUARE) of hyperpolarized (83)Kr. *Magn Reson Imaging* 32(1):48–53.
24. Lilburn DML, et al. (2015) Hyperpolarized 83Kr magnetic resonance imaging of alveolar degradation in a rat model of emphysema. *J R Soc Interface* 12(107):20150192.
25. Comment A, et al. (2010) Hyperpolarizing gases via dynamic nuclear polarization and sublimation. *Phys Rev Lett* 105(1):018104.
26. Capozzi A, Roussel C, Comment A, Hyacinthe JN (2015) Optimal glass-forming solvent brings sublimation dynamic nuclear polarization to Xe-129 hyperpolarization biomedical imaging standards. *J Phys Chem C* 119(9):5020–5025.
27. Happer W (1972) Optical pumping. *Rev Mod Phys* 44(2):169–249.
28. Wagshul ME, Chupp TE (1989) Optical pumping of high-density Rb with a broadband dye laser and GaAlAs diode laser arrays: Application to 3He polarization. *Phys Rev A* 40(8):4447–4454.
29. Kuzma NN, Patton B, Raman K, Happer W (2002) Fast nuclear spin relaxation in hyperpolarized solid 129Xe. *Phys Rev Lett* 88(14):147602.
30. Baumer D, Brunner E, Blümler P, Zänker PP, Spiess HW (2006) NMR spectroscopy of laser-polarized (129)Xe under continuous flow: A method to study aqueous solutions of biomolecules. *Angew Chem Int Ed Engl* 45(43):7282–7284.
31. Cleveland ZI, Möller HE, Hedlund LW, Driehuys B (2009) Continuously infusing hyperpolarized 129Xe into flowing aqueous solutions using hydrophobic gas exchange membranes. *J Phys Chem B* 113(37):12489–12499.
32. Duewel M, et al. (2012) Online monitoring of styrene polymerization in miniemulsion by hyperpolarized (129)xenon NMR spectroscopy. *Macromolecules* 45(4):1839–1846.
33. Imai H, et al. (2015) Regional fractional ventilation mapping in spontaneously breathing mice using hyperpolarized ^{129}Xe MRI. *NMR Biomed* 28(1):24–29.
34. Norquay G, et al. (2015) Relaxation and exchange dynamics of hyperpolarized 129Xe in human blood. *Magn Reson Med* 74(2):303–311.
35. Causier A, Carret G, Boutin C, Berthelot T, Berthault P (2015) 3D-printed system optimizing dissolution of hyperpolarized gaseous species for micro-sized NMR. *Lab Chip* 15(9):2049–2054.
36. Witte C, et al. (2015) Live-cell MRI with xenon hyper-CEST biosensors targeted to metabolically labeled cell-surface glycans. *Angew Chem Int Ed Engl* 54(9):2806–2810.
37. Wang Y, Dmochowski IJ (2015) Cucurbit[6]uril is an ultrasensitive (129)Xe NMR contrast agent. *Chem Commun (Camb)* 51(43):8982–8985.
38. Tassali N, et al. (2014) Smart detection of toxic metal ions, Pb2+ and Cd2+, using a 129Xe NMR-based sensor. *Anal Chem* 86(3):1783–1788.
39. Six JS, Hughes-Riley T, Stupic KF, Pavlovskaya GE, Meersmann T (2012) Pathway to cryogen free production of hyperpolarized Krypton-83 and Xenon-129. *PLoS One* 7(11):e49927.
40. Hughes-Riley T, et al. (2013) Cryogenics free production of hyperpolarized 129Xe and 83Kr for biomedical MRI applications. *J Magn Reson* 237:23–33.
41. Nikolaou P, et al. (2014) A 3D-printed high power nuclear spin polarizer. *J Am Chem Soc* 136(4):1636–1642.
42. Hrycyshyn ES, Krause L (1970) Inelastic collisions between excited alkali atoms and molecules. 7. Sensitized fluorescence and quenching in mixtures of rubidium with H2, HD, N2, CD4, C2H2, and C2H6. *Can J Phys* 48(22):2761–2768.
43. Young L, Holt RJ, Green MC, Kowalczyk RS (1989) Laser-driven polarized sources of hydrogen and deuterium. *Nucl Phys A* 497:C529–C533.
44. Redsun SG, Knize RJ, Cates GD, Happer W (1990) Production of highly spin-polarized atomic hydrogen and deuterium by spin-exchange optical pumping. *Phys Rev A* 42(3): 1293–1301.
45. Anderson LW, Walker T (1992) The effect of radiation trapping on a high-field spin exchange optically pumped target. *Nucl Instr Meth Phys Res A* 316(2-3):123–127.
46. Anderson LW, Walker T (1995) Spin-exchange optical-pumping of hydrogen and deuterium nuclei. *Nucl Instr Meth Phys Res A* 357(2-3):220–224.
47. Tam A, Moe G, Happer W (1975) Particle formation by resonant laser light in alkali-metal vapor. *Phys Rev Lett* 35(24):1630–1633.
48. Volk CH, Kwon TM, Mark JG, Kim YB, Woo JC (1980) Measurement of the Rb-Xe-131 spin-exchange cross-section in Xe-131 relaxation studies. *Phys Rev Lett* 44(3):136–139.
49. Kwon TM, Mark JG, Volk CH (1981) Quadrupole nuclear-spin relaxation of Xe-131 in the presence of rubidium vapor. *Phys Rev A* 24(4):1894–1903.
50. Wu Z, Happer W, Kitano M, Daniels J (1990) Experimental studies of wall interactions of adsorbed spin-polarized 131Xe nuclei. *Phys Rev A* 42(5):2774–2784.
51. Rohrbaugh S, Wang HTJ, Singh J, Tobias WA, Cates GD (2012) Magnetic decoupling of Xe-129 nuclear spin relaxation due to wall collisions with RbH and RbD coatings. *Phys Rev A* 86(4):043413.
52. Rosenberry MA, Reyes JP, Tupa D, Gay TJ (2007) Radiation trapping in rubidium optical pumping at low buffer-gas pressures. *Phys Rev A* 75(2).
53. Zameroski ND, Rudolph W, Hager GD, Hostutler DA (2009) A study of collisional quenching and radiation-trapping kinetics for Rb(5p) in the presence of methane and ethane using time-resolved fluorescence. *J Phys At Mol Opt Phys* 42(24):245401.
54. Stupic KF, Six JS, Olsen MD, Pavlovskaya GE, Meersmann T (2013) Combustion resistance of the 129Xe hyperpolarized nuclear spin state. *Phys Chem Chem Phys* 15(1): 94–97.
55. Cleveland ZI, et al. (2007) Hyperpolarized 83Kr and 129Xe NMR relaxation measurements of hydrated surfaces: Implications for materials science and pulmonary diagnostics. *J Am Chem Soc* 129(6):1784–1792.
56. Stupic KF, Cleveland ZI, Pavlovskaya GE, Meersmann T (2006) Quadrupolar relaxation of hyperpolarized krypton-83 as a probe for surfaces. *Solid State Nucl Magn Reson* 29(1-3):79–84.
57. Chen LM, Yang XG, Li X, Li G, Snape C (2015) Prediction of formation of gas-phase bubbles correlated by vortices in the fuel reactor of chemical looping combustion. *Fuel Process Technol* 130:235–244.
58. Anger BC, et al. (2008) Gas-phase spin relaxation of Xe-129. *Phys Rev A* 78(4):043406.
59. Berry-Pusey BN, Anger BC, Laicher G, Saam B (2006) Nuclear spin relaxation of Xe-129 due to persistent xenon dimers. *Phys Rev A* 74(6):063408.
60. Repetto M, et al. (2015) Systematic T1 improvement for hyperpolarized 129xenon. *J Magn Reson* 252:163–169.
61. Stupic KF, Cleveland ZI, Pavlovskaya GE, Meersmann T (2011) Hyperpolarized (131)Xe NMR spectroscopy. *J Magn Reson* 208(1):58–69.